Inorganic Chemistry

ARTICLE

pubs.acs.org/IC

Studies of a Series of $[Ni(P^R_2N^{Ph}_2)_2(CH_3CN)]^{2+}$ Complexes as Electrocatalysts for H_2 Production: Substituent Variation at the Phosphorus Atom of the P_2N_2 Ligand

Uriah J. Kilgore,[†] Michael P. Stewart,[†] Monte L. Helm,[†,‡,∥] William G. Dougherty,[§] W. Scott Kassel,[§] Mary Rakowski DuBois,[†] Daniel L. DuBois,*[,†] and R. Morris Bullock*[,†]

[†]Center for Molecular Electrocatalysis, Pacific Northwest National Laboratory, P.O. Box 999, K2-57, Richland, Washington 99352, United States

[‡]Department of Chemistry, Fort Lewis College, Durango, Colorado 81301

[§]Department of Chemistry, Villanova University, Villanova, Pennsylvania 19085, United States

Supporting Information

ABSTRACT: A series of $[Ni(P^R_2N^{Ph}_2)_2(CH_3CN)](BF_4)_2$ complexes containing the cyclic diphosphine ligands $[P^R_2N^{Ph}_2$ = 1,5-diaza-3,7-diphosphacyclooctane; R = benzyl (Bn), *n*-butyl (*n*-Bu), 2-phenylethyl (PE), 2,4,4-trimethylpentyl (TP), and cyclohexyl (Cy)] have been synthesized and characterized. X-ray diffraction studies reveal that the cations of $[Ni(P^{Bn}_2N^{Ph}_2)_2(CH_3CN)](BF_4)_2$ and $[Ni(P^{n\text{-}Bu}_2N^{Ph}_2)_2(CH_3CN)](BF_4)_2$ have distorted trigonal bipyramidal geometries. The Ni(0) complex $[Ni(P^{Bn}_2N^{Ph}_2)_2]$ was also synthesized and characterized by X-ray diffraction studies and shown to have a distorted tetrahedral structure. These complexes, with the exception of $[Ni(P^{Cy}_2N^{Ph}_2)_2(CH_3CN)](BF_4)_2$, all exhibit reversible electron transfer processes for both the Ni(II/I) and Ni(I/0) couples and are electrocatalysts for the production of H_2 in acidic acetonitrile solutions. The heterolytic cleavage of H_2 by $[Ni(P^R_2N^{Ph}_2)_2(CH_3CN)](BF_4)_2$ complexes in the presence of *p*-anisidine or *p*-bromoaniline was used to determine the hydride donor abilities of the corresponding $[HNi(P^R_2N^{Ph}_2)_2](BF_4)$ complexes. However, for the catalysts with the most bulky R groups, the turnover frequencies do not parallel the driving force for elimination of H_2, suggesting that steric interactions between the alkyl substituents on phosphorus and the nitrogen atom of the pendant amines play an important role in determining the overall catalytic rate.

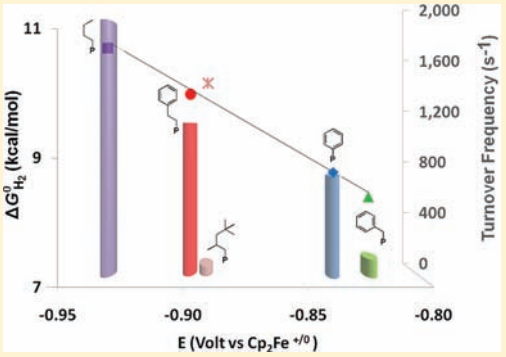

INTRODUCTION

Renewable energy sources such as solar and wind have the potential to significantly reduce fossil fuel consumption, but the intermittent nature of electricity generated from these sources makes efficient storage of this energy critical.[1] An attractive option is to store the excess energy available during peak production in the form of fuels with a high energy density, such as H_2. In order to use H_2 on a large scale, inexpensive electrocatalysts that are capable of efficiently converting electrical energy into chemical bonds are needed. In nature, hydrogenase enzymes carry out oxidation of H_2 and reduction of H^+ to produce H_2.[2] The active sit11es of these enzymes contain nickel and iron, and these have inspired attempts to develop synthetic complexes as structural models capable of mimicking the functions of hydrogenases.[3]

Previous studies from our laboratories have shown that $[Ni(P^R_2N^{R'}_2)_2(CH_3CN)]^{2+}$ complexes (where $P^R_2N^{R'}_2$ is a 1, 5-diaza-3,7-diphosphacyclooctane ligand) are highly active electrocatalysts for oxidation of H_2 or reduction of H^+ to produce H_2.[4−9] Comparison of these $[Ni(P^R_2N^{R'}_2)_2(CH_3CN)]^{2+}$ complexes to other bis(diphosphine) complexes of nickel clearly demonstrates that the pendant amines dramatically accelerate one or more of the elementary steps in the catalytic cycle. Additionally, the simple synthesis of $P^R_2N^{R'}_2$ ligands permits easy modification of the substituents on P and N, and, thus, both the first and second coordination spheres of these catalysts. Previous work by our group has examined the effects of varying the basicity of the proton relay, a second coordination sphere component. It was demonstrated that varying the *p*-substituent of the aniline-based pendant amine affected both the redox properties and the thermodynamic driving force for H_2 production, and ultimately the turnover frequency of the catalyst.[8] The work presented here examines the consequences of varying the substituents at the phosphorus atoms of the 1,5-diaza-3,7-diphosphacyclooctane $(P^R_2N^{Ph}_2)$ ligands in nickel catalysts for H_2 production.

RESULTS

Synthesis and Characterization of Ligands and Nickel Complexes. Most of the new and previously reported ligands

Received: July 10, 2011
Published: October 14, 2011

Scheme 1. Synthesis of $(P^{R}{}_2N^{Ph}{}_2)$ Ligands and $[Ni(P^{R}{}_2N^{Ph}{}_2)_2(CH_3CN)]^{2+}$ Complexes

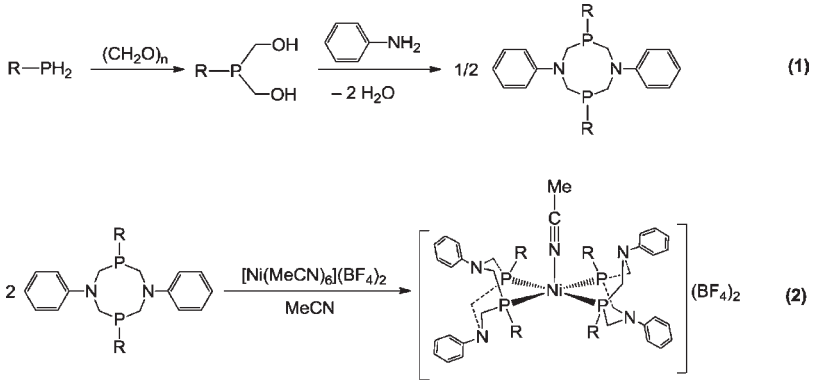

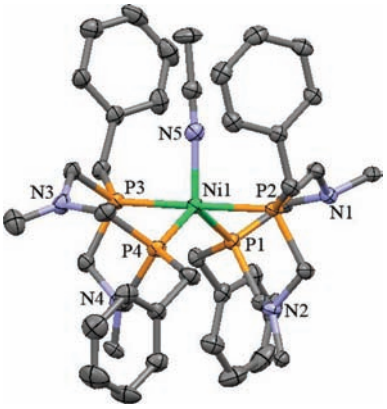

Figure 1. Structure of the $[Ni(P^{Bn}{}_2N^{Ph}{}_2)_2(CH_3CN)]^{2+}$ cation. BF_4 anions and THF molecules are omitted, and only the *ipso* carbon atoms of the phenyl groups on the N atom are shown for clarity. Thermal ellipsoids are plotted at the 50% confidence level.

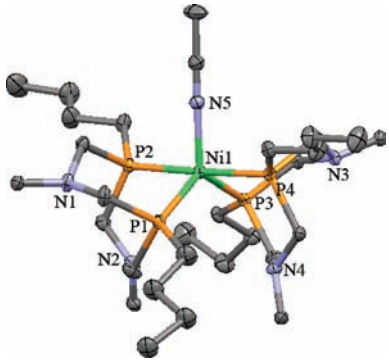

Figure 2. Structure of the $[Ni(P^{n\text{-}Bu}{}_2N^{Ph}{}_2)_2(CH_3CN)]^{2+}$ cation. BF_4 anions and THF molecules are omitted, and only the *ipso* carbon atoms of the phenyl groups on the N atom are shown for clarity. Thermal ellipsoids are plotted at the 50% confidence level.

used in this study were prepared using a single-flask two-step reaction (reaction 1 in Scheme 1). In the first step, a primary phosphine, RPH_2, where R = benzyl (Bn), *n*-butyl (*n*-Bu), 2-phenylethyl (PE), 2,4,4-trimethylpentyl (TP), or cyclohexyl, was treated with 2 equiv of paraformaldehyde to form the corresponding bis(hydroxymethyl)phosphine (reaction 1 of Scheme 1). This product was dissolved in hot ethanol, and then treated with an equivalent of aniline. The diazadiphosphacyclooctane $(P^{R}{}_2N^{Ph}{}_2)$ ligands were isolated as white solids and have $^{31}P\{^1H\}$ NMR chemical shifts between −46 and −53 ppm, comparable to $P^{Ph}{}_2N^{C6H4X}{}_2$ ligands reported previously.[8] ^1H NMR spectral data and mass spectrometric data are also consistent with formation of 1,5-diaza-3,7-diphosphacyclooctane $(P^{R}{}_2N^{Ph}{}_2)$ ligands (see Experimental Section for details).

The $[Ni(P^{R}{}_2N^{Ph}{}_2)_2(CH_3CN)](BF_4)_2$ complexes were prepared by addition of 2 equiv of the diazadiphosphacyclooctane ligands to an acetonitrile solution of $[Ni(CH_3CN)_6](BF_4)_2$. The NMR and mass spectra data are consistent with the structures shown in reaction 2 in Scheme 1. The $^{31}P\{^1H\}$ NMR spectra of these complexes all consist of a single resonance between 5 and 9 ppm, 47−62 ppm downfield of the free ligand resonances. Complexation results in bicyclic diphosphine ligands that exhibit rapid boat−chair interconversion of the six-membered chelate rings, and two multiplets in the ^1H NMR spectra between 3.99 and 3.44 ppm are characteristic of the diastereotopic methylene protons. X-ray diffraction studies of two of these complexes have been performed as described in the next paragraph, and additional data supporting the formulations of these complexes is provided in the Experimental Section.

Dark red crystals of $[Ni(P^{Bn}{}_2N^{Ph}{}_2)_2(CH_3CN)](BF_4)_2$ and $[Ni(P^{n\text{-}Bu}{}_2N^{Ph}{}_2)_2(CH_3CN)](BF_4)_2$ were grown by vapor diffusion of hexane into a THF solution containing a few drops of acetonitrile. For $[Ni(P^{Bn}{}_2N^{Ph}{}_2)_2(CH_3CN)](BF_4)_2$ the unit cell consisted of a discrete dication, two tetrafluoroborate anions, and disordered THF and acetonitrile solvent molecules. For $[Ni(P^{n\text{-}Bu}{}_2N^{Ph}{}_2)_2(CH_3CN)](BF_4)_2$ the crystals consist of a discrete dication, two tetrafluoroborate anions, three THF molecules, and one acetonitrile solvent molecule. The nickel cations are depicted in Figures 1 and 2, and selected bond lengths and angles are given in Tables 1 and 2 for $[Ni(P^{Bn}{}_2N^{Ph}{}_2)_2(CH_3CN)](BF_4)_2$ and $[Ni(P^{n\text{-}Bu}{}_2N^{Ph}{}_2)_2(CH_3CN)](BF_4)_2$, respectively. The structures are best described as trigonal bipyramids having two axial and two equatorial phosphines, with the acetonitrile ligand occupying the third equatorial position. The Ni−P bond lengths of 2.17−2.21 Å are typical for Ni(II) complexes with bidentate phosphine ligands, and the P−Ni−P bite angles of 80−82° for the diphosphine ligands are also in the normal range observed for this class of complexes.[6,8] For both complexes the two six-membered rings adjacent to the coordinated acetonitrile ligand

dx.doi.org/10.1021/ic201461a |*Inorg. Chem.* 2011, 50, 10908–10918

Table 1. Selected Bond Distances and Angles for $[Ni(P^{Bn}{}_2N^{Ph}{}_2)_2(CH_3CN)](BF_4)_2$

bond distance (Å)		bond angle (deg)	
Ni(1)−P(1)	2.2050(8)	P(1)−Ni(1)−P(3)	98.92(3)
Ni(1)−P(2)	2.1909(7)	P(1)−Ni(1)−P(2)	80.28(3)
Ni(1)−P(3)	2.2051(7)	P(3)−Ni(1)−P(2)	178.52(3)
Ni(1)−P(4)	2.2137(7)	P(1)−Ni(1)−P(4)	122.80(3)
Ni(1)−N(5)	1.975(2)	P(3)−Ni(1)−P(4)	82.16(3)
		P(2)−Ni(1)−P(4)	99.32(3)

Table 2. Selected Bond Distances and Angles for $[Ni(P^{n\text{-}Bu}{}_2N^{Ph}{}_2)_2(CH_3CN)](BF_4)_2$

bond distance (Å)		bond angle (deg)	
Ni(1)−P(1)	2.2124(5)	P(1)−Ni(1)−P(3)	119.81(2)
Ni(1)−P(2)	2.1775(5)	P(1)−Ni(1)−P(2)	82.68(2)
Ni(1)−P(3)	2.1898(5)	P(3)−Ni(1)−P(2)	100.49(2)
Ni(1)−P(4)	2.1672(5)	P(1)−Ni(1)−P(4)	98.48(2)
Ni(1)−N(5)	1.9859(16)	P(3)−Ni(1)−P(4)	81.046(19)
		P(2)−Ni(1)−P(4)	177.33(2)

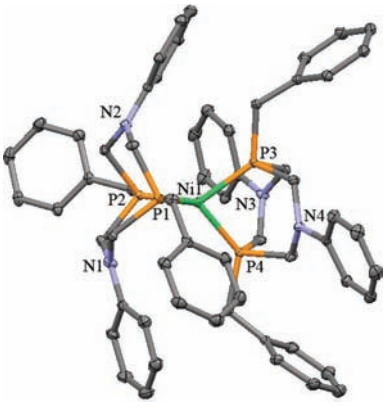

Figure 3. Structure of $Ni(P^{Bn}{}_2N^{Ph}{}_2)_2$. Thermal ellipsoids plotted at 50% confidence level.

adopt chair conformations to minimize steric interactions with acetonitrile, and the other two six-membered rings adopt boat conformations. This results in Ni···N(2) and Ni···N(1) distances of 3.423 and 3.830 Å, respectively, for $[Ni(P^{Bn}{}_2N^{Ph}{}_2)_2(CH_3CN)](BF_4)_2$, and Ni···N(2) and Ni···N(1) distances of 3.371 and 3.811 Å, respectively, for $[Ni(P^{n\text{-}Bu}{}_2N^{Ph}{}_2)_2(CH_3CN)](BF_4)_2$.

The Ni(0) complex $Ni(P^{Bn}{}_2N^{Ph}{}_2)_2$ was synthesized by reducing $[Ni(P^{Bn}{}_2N^{Ph}{}_2)_2(CH_3CN)](BF_4)_2$ under an atmosphere of H_2 in the presence of excess base, tetramethylguanidine. In the ^{31}P NMR spectrum of the product, a singlet at −1.03 ppm is assigned to the equivalent phosphorus atoms, as expected for a tetrahedral structure.

Large yellow crystals of $Ni(P^{Bn}{}_2N^{Ph}{}_2)_2$ suitable for X-ray diffraction studies were grown by slow evaporation of an acetonitrile solution. The structure of the Ni(0) complex is depicted in Figure 3, and selected bond lengths and angles are given in Table 3. The coordination geometry is a distorted tetrahedron with a dihedral angle between ligands of 78.5°. The P−Ni−P bite

Table 3. Selected Bond Distances and Angles for $Ni(P^{Bn}{}_2N^{Ph}{}_2)_2$

bond distance (Å)		bond angle (deg)	
Ni(1)−P(1)	2.1376(3)	P(1)−Ni(1)−P(3)	116.510(11)
Ni(1)−P(2)	2.1485(3)	P(1)−Ni(1)−P(2)	85.412(11)
Ni(1)−P(3)	2.1431(3)	P(3)−Ni(1)−P(2)	128.726(11)
Ni(1)−P(4)	2.1351(3)	P(1)−Ni(1)−P(4)	129.640(11)
		P(3)−Ni(1)−P(4)	85.297(11)
		P(2)−Ni(1)−P(4)	116.869(11)

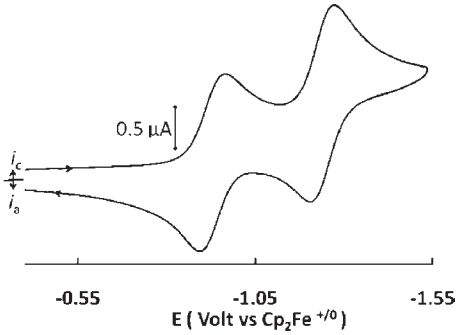

Figure 4. Cyclic voltammogram of 1 mM $[Ni(P^{n\text{-}Bu}{}_2N^{Ph}{}_2)_2(CH_3CN)](BF_4)_2$ in acetonitrile/0.2 M NEt_4BF_4 with a 1 mm glassy carbon working electrode; scan rate = 0.1 V s^{-1}.

angles of ∼85° are 2−4° larger than those observed for the trigonal bipyramidal Ni(II) complexes. This is attributed to a preference of Ni(0) complexes for a 109° P−Ni−P bond angle compared to a 90° P−Ni−P angle in an ideal trigonal bipyramid and a shorter Ni−P bond distance of 2.14 Å. For this complex, all of the six-membered rings adopt a boat conformation, although a mixture of chair and boat conformations is likely present in solution.[10] The Ni···N distances range from 3.34 to 3.53 Å.

Electrochemical Studies of $[Ni(P^{R}{}_2N^{Ph}{}_2)_2(CH_3CN)](BF_4)_2$ Complexes. With the exception of $[Ni(P^{Cy}{}_2N^{Ph}{}_2)_2(CH_3CN)]^{2+}$, cyclic voltammograms of each Ni(II) complex in this study exhibit two distinct and reversible reduction waves assigned to the Ni(II/I) and Ni(I/0) couples in acetonitrile. A typical voltammogram is shown in Figure 4 (voltammograms for all complexes are given in the Supporting Information). Plots of the peak current (i_p) versus $v^{1/2}$ are linear for both reduction waves, indicating that these reductions are diffusion-controlled.[11] For $[Ni(P^{Cy}{}_2N^{Ph}{}_2)_2(CH_3CN)]^{2+}$, the Ni(I/0) reduction is irreversible in acetonitrile (Figure S1) but reversible in benzonitrile (Figure S3). The irreversible Ni(I/0) couple in acetonitrile is attributed to the poor solubility of the Ni(0) complex in acetonitrile which causes it to adsorb on the electrode. The cyclic voltammogram of $Ni(P^{Bn}{}_2N^{Ph}{}_2)_2$ in benzonitrile shows a quasireversible one-electron redox wave for the Ni(II/I) couple and a reversible redox wave for the Ni(I/0) couple. Identical electrochemical behavior is observed for $[Ni(P^{Bn}{}_2N^{Ph}{}_2)_2(CH_3CN)]^{2+}$ in benzonitrile. Redox potentials ($E_{1/2}$ reported vs $Cp_2Fe^{+/0}$ at 0.00 V), peak-to-peak separations (ΔE_p, v = 100 mV s^{-1}), and the differences in the Ni(II/I) and Ni(I/0) couples ($\Delta E_{1/2}$) are given in Table 4 for all of the $[Ni(P^{R}{}_2N^{Ph}{}_2)_2(CH_3CN)]^{2+}$ complexes.

Thermodynamic Properties of $[Ni(P^{R}{}_2N^{Ph}{}_2)_2(CH_3CN)]^{2+}$ and $[HNi(P^{R}{}_2N^{Ph}{}_2)_2]^{+}$ Complexes. Hydride donor abilities were

dx.doi.org/10.1021/ic201461a |*Inorg. Chem.* 2011, 50, 10908–10918

Table 4. Electrochemical Data for $[Ni(P^R_2N^{Ph}_2)_2(CH_3CN)]^{2+}$ Complexes in Acetonitrile (0.2 M NEt_4BF_4) Referenced to $Cp_2Fe^{+/0}$

	Ni(II/I)		Ni(I/0)		
R	$E_{1/2}$ (V)	ΔE_p (mV)	$E_{1/2}$ (V)	ΔE_p (mV)	$\Delta E_{1/2}$ (mV)
n-butyl (*n*-Bu)	−0.93	68	−1.23	65	300
2-phenylethyl (PE)	−0.90	65	−1.16	65	260
2,4,4-trimethylpentyl (TP)	−0.89	69	−1.17	62	280
phenyl (Ph)	−0.84	69	−1.02	73	180
benzyl (Bn)	−0.83	72	−1.12	66	290
cyclohexyl (Cy)[a]	−0.60	75	−1.12	81	520

[a] Benzonitrile solvent.

Scheme 2. Thermodynamic Cycle for Determination of ΔG°_{H-}

$$[HNi(P^R_2N^{R'}_2)_2]^+ + BH^+ \rightleftharpoons [Ni(P^R_2N^{R'}_2)_2]^{2+} + H_2 + B \quad (3) \quad -RT\ln K$$

$$B + H^+ \rightleftharpoons BH^+ \quad (4) \quad -1.364pKa$$

$$H_2 \rightleftharpoons H^+ + H^- \quad (5) \quad 76\ kcal/mol$$

$$[HNi(P^R_2N^{R'}_2)_2]^+ \rightleftharpoons [Ni(P^R_2N^{R'}_2)_2]^{2+} + H^- \quad \Delta G^\circ_{H-}$$

$$\Delta G^\circ_{H-} = -RT\ln K - 1.364pKa + 76.0\ kcal/mol \quad (6)$$

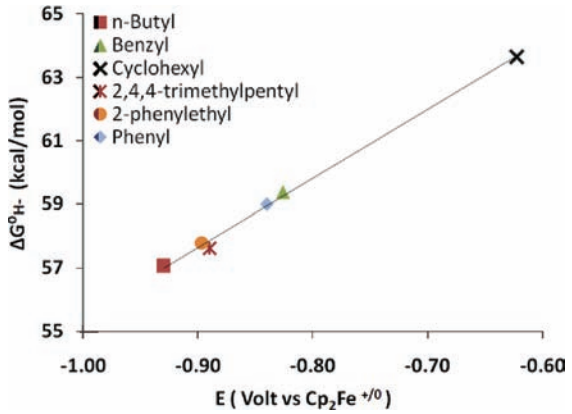

Figure 5. Plot of hydride donor abilities as a function of $E_{1/2}$ of the Ni(II/I) couple for all complexes listed. Line fit equation: $\Delta G^\circ_{H-} = 21.7\ E_{1/2}$ Ni(II/I) + 77.2; $R^2 = 0.997$.

calculated for $[HNi(P^R_2N^{Ph}_2)_2]^+$ complexes from the thermochemical cycle shown in Scheme 2, by measuring equilibrium constants for heterolysis of H_2 to generate $[HNi(P^R_2N^{Ph}_2)_2]^+$ using *p*-anisidine or *p*-bromoaniline as the base (B) in acetonitrile (Scheme 2, the reverse of reaction 3). The Ni(II) complexes discussed here do not add H_2 (P_{H_2} = 1 atm) in the absence of an external base. The equilibrium constants for reaction 3 in Scheme 2 were determined by ^{31}P and ^1H NMR spectroscopy as described in the Experimental Section. In eq 5 of Scheme 2, 76.0 kcal/mol is the free energy for heterolytic cleavage of H_2 in acetonitrile.[12] These equilibrium constants, the pK_a values of the protonated base (BH^+), and the free energy for heterolytic H_2 cleavage are used in eq 6 of Scheme 2 to calculate the free energies (ΔG°_{H-}) for the heterolytic cleavage of the Ni−H bond in acetonitrile. This method for determining hydride donor abilities is discussed in more detail elsewhere.[13,14]

Scheme 3. Thermodynamic Cycle for Estimation of ΔG°_{H2}

$$[Ni(P^R_2N^{R'}_2)_2]^{2+} + H^- \rightleftharpoons [HNi(P^R_2N^{R'}_2)_2]^+ \quad (7) \quad -\Delta G^\circ_{H-}$$

$$[HNi(P^R_2N^{R'}_2)_2]^+ + H^+ \rightleftharpoons [HNi(P^R_2HN^{R'}_2)(P^R_2N^{R'}_2)]^{2+} \quad (8) \quad -1.364pK_a$$

$$H_2 \rightleftharpoons H^+ + H^- \quad (9) \quad 76\ kcal/mol$$

$$[Ni(P^R_2N^{R'}_2)_2]^{2+} + H_2 \rightleftharpoons [HNi(P^R_2HN^{R'}_2)(P^R_2N^{R'}_2)]^{2+} \quad (10) \quad \Delta G^\circ_{H2}$$

$$\Delta G^\circ_{H2} = -\Delta G^\circ_{H-} - 1.364pK_a + 76.0\ kcal/mol \quad (11)$$

Table 5. Thermochemical Data for $[HNi(P^R_2N^{Ph}_2)_2]^+$ Complexes

R	ΔG°_{H-} (kcal/mol)[a]	ΔG°_{H2} (kcal/mol)[b]
n-butyl	57.1	10.7
2-phenylethyl	57.8	10.0
2,4,4-trimethylpentyl	57.6	10.2
phenyl	59.0[13]	8.8
benzyl	59.4	8.4
cyclohexyl	63.7[15]	4.1

[a] Hydride donor ability (eq 6). [b] Free energy for H_2 binding to $[Ni(P^R_2N^{Ph}_2)_2(CH_3CN)]^+$ complexes; see Scheme 3 and Supporting Information.

A plot of ΔG°_{H-} for the $[HNi(P^R_2N^{Ph}_2)_2]^+$ complexes versus the potential of the Ni(II/I) couple for the corresponding $[Ni(P^R_2N^{Ph}_2)_2(CH_3CN)]^{2+}$ complexes is linear, as shown in Figure 5. The hydride donor ability decreases (ΔG°_{H-} becomes more positive) as the Ni(II/I) redox potential becomes more positive. Similar correlations have been reported previously for other $[HNi(diphosphine)_2]^+$ complexes.[16,17] Protonation of the Ni(II) hydride complex in acetonitrile leads to the formation of $[Ni^0(P^{Ph}_2N^{Ph}N^{Ph}H)_2]^{2+}$ (Scheme 3), for which a pK_a value of 6.0 has been estimated.[13,18] As shown in Scheme 3, the hydride donor abilities and pK_a data can be used to calculate free energies for H_2 binding and cleavage by the corresponding $[Ni^{II}(P^R_2N^{Ph}_2)(CH_3CN)]^{2+}$ complexes (ΔG°_{H2}; Table 5). Larger positive values of ΔG°_{H2} indicate a more favorable driving force for H−H bond formation and elimination of H_2 from diprotonated intermediates during the catalytic cycle for H_2 production.

Electrocatalytic Properties of $[Ni(P^R_2N^{Ph}_2)_2(CH_3CN)](BF_4)_2$ Complexes. Figure 6 shows a series of cyclic voltammograms for $[Ni(P^{n\text{-}Bu}_2N^{Ph}_2)_2(CH_3CN)](BF_4)_2$ in the presence of increasing

dx.doi.org/10.1021/ic201461a |*Inorg. Chem.* 2011, 50, 10908–10918

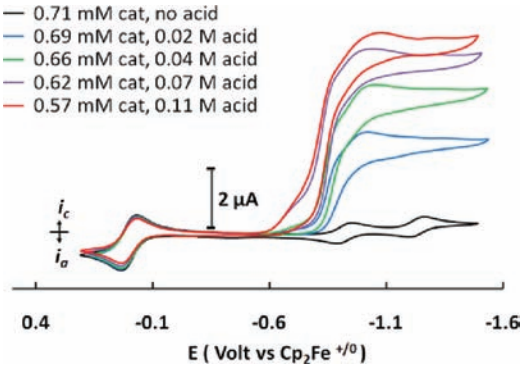

Figure 6. Cyclic voltammograms of 0.7 mM $[Ni(P^{n\text{-}Bu}{}_2N^{Ph})_2(CH_3CN)](BF_4)_2$ in acetontrile/0.2 M Et_4NBF_4 with a 1 mm glassy carbon working electrode and internal ferrocene reference; scans taken in absence of acid (black) and in the presence of various concentrations of acid ([(DMF)H]OTf). Scan rate = 0.05 V s^{-1}.

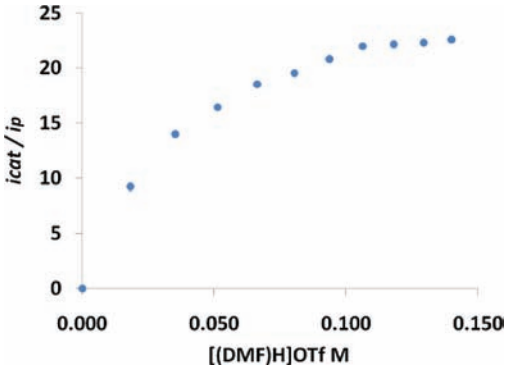

Figure 7. Plot of i_{cat}/i_p vs [acid] for $[Ni(P^{n\text{-}Bu}{}_2N^{Ph}{}_2)_2(CH_3CN)](BF_4)_2$ catalyst in acetonitrile/0.2 M Et_4NBF_4 with a 1 mm glassy carbon working electrode in the presence of [(DMF)H]OTf.

concentrations of protonated dimethylformamide, [(DMF)-H]OTf, as the acid (pK_a^{MeCN} = 6.1).[19] The black trace corresponds to the complex in the absence of acid and consists of reversible waves for the Ni(II/I) and Ni(I/0) couples. The wave at 0.0 V is that of the ferrocenium/ferrocene couple resulting from the addition of ferrocene as an internal standard. The colored traces are for cyclic voltammograms recorded in the presence of increasing acid concentrations as indicated in the figure legend. The small decrease in catalyst concentrations reflects dilution due to addition of aliquots of acid solution. The value of i_p (vide infra) is corrected for dilution when determining the turnover frequency. It can be seen that there is a significant increase in the current near the Ni(II/I) couple as increasing amounts of acid are added. In addition, the waves assume a plateau shape expected for catalysts operating in the presence of excess acid substrate. At higher acid concentrations, the waves are shifted to potentials that are positive of the Ni(II/I) couple in the absence of acid. For the red trace (0.11 M acid) the potential at the half-height of the catalytic wave is shifted positive by 130 mV. This observation is consistent with protonation of the Ni(I) species formed upon reduction of Ni(II) at a rate that is significantly faster than the overall catalytic rate. Under these conditions, the half-wave potential of the Ni(II/I) couple is influenced by the rate of the following protonation reaction, but the current is determined by the overall catalytic rate. Slight changes in slope in the red trace suggest that there may be as many as three different protonation events that influence the catalytic potential. As discussed below, these may represent different sites of protonation of the catalyst. Hydrogen production for $[Ni(P^{PE}{}_2N^{Ph}{}_2)_2(CH_3CN)]^{2+}$ and $[Ni(P^{n\text{-}Bu}{}_2N^{Ph}{}_2)_2(CH_3CN)]^{2+}$ was confirmed by gas chromatographic analysis of the headspace gas obtained in a bulk electrolysis experiment. The current efficiency determined for the $[Ni(P^{PE}{}_2N^{Ph}{}_2)_2(CH_3CN)]^{2+}$ catalyst was found to be 95 ± 5%.

Figure 7 shows the ratio (i_{cat}/i_p) of the catalytic current (i_{cat}) to the peak current (i_p) for the Ni(II/I) couple observed in the absence of acid. This ratio increases as the acid concentration increases up to 0.11 M acid, and at still higher concentrations the ratio becomes constant. In general, this is the behavior expected for a catalyst that saturates with substrate. Equation 12 can be used to calculate a turnover frequency (TOF) of 46 s^{-1} for $[Ni(P^{n\text{-}Bu}{}_2N^{Ph})_2(CH_3CN)](BF_4)$ in the acid independent region.[7,20]

Table 6. Turnover Frequencies and Overpotentials for Proton Reduction in Acetonitrile.

	turnover frequencies (s^{-1}) and overpotentials (mV)[a]			
	[(DMF)H]OTf		[cyanoanilinium]OTf	
R	without water	with water	without water	with water
n-butyl	46	1820	4	214
	(450)	(500)	(330)	(440)
2-phenylethyl	31	1080	11	141
	(330)	(450)	(290)	(310)
2,4,4-trimethylpentyl	<1	69	<1	19
	(360)	(450)	(280)	(400)
phenyl[b]	590	720	28	72
	(300)	(320)	(270)	(330)
benzyl	7	130	3	28
	(410)	(460)	(230)	(320)

[a] Overpotentials in mV are indicated in parentheses. Determined using the method of Evans et al.[21] [b] Previously determined,[8] included for comparison.

Similar studies were carried out for the 2-phenylethyl and benzyl derivatives using [(DMF)H]OTf as the acid, and their turnover frequencies are listed in Table 6. The overpotentials calculated according to the method of Evans et al. are also listed in Table 6.[21]

$$\frac{i_{cat}}{i_p} = \frac{n}{0.4463}\sqrt{\frac{RTk_{obs}}{Fv}} \qquad (12)$$

Evaluation of $[Ni(P^{Cy}{}_2N^{Ph}{}_2)_2(CH_3CN)]^{2+}$ as a catalyst for hydrogen production was precluded by its decomposition in acidic solutions, and $[Ni(P^{TP}{}_2N^{Ph}{}_2)_2(CH_3CN)]^{2+}$ is a significantly slower catalyst than the other derivatives in the presence of >0.10 M $[(DMF)H]^+OTf^-$, as can be seen by comparing the cyclic voltammograms in Figure 8 with those in Figure 6. The shift in the potential of the Ni(II/I) wave in the absence of acid (black trace) to more positive potentials in the presence of acid (red trace) indicates that, following reduction of Ni(II), protonation of the Ni(I) species is rapid. However, catalysis is slow, as indicated by the small increase in current in the presence of a large excess of acid. We estimate that the catalytic

dx.doi.org/10.1021/ic201461a |*Inorg. Chem.* 2011, 50, 10908–10918

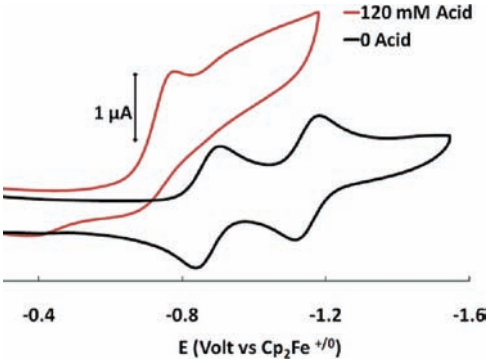

Figure 8. Cyclic voltammograms of 0.7 mM $[Ni(P^{TP}{}_2N^{Ph})_2(CH_3CN)](BF_4)_2$ in acetonitrile/0.2 M Et_4NBF_4 with a 1 mm glassy carbon working electrode; scans taken in the absence of (black) and in the presence (red) of 120 mM acid ([(DMF)H]OTf). Scan rate = 0.1 V s^{-1}.

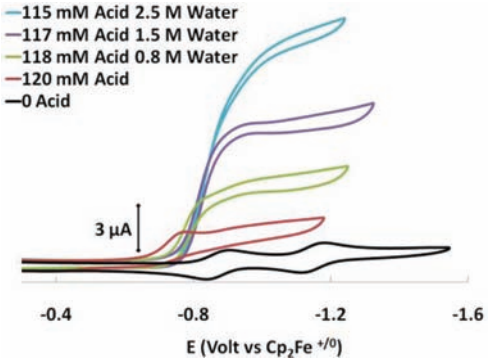

Figure 9. Cyclic voltammograms of 0.7 mM $[Ni(P^{TP}{}_2N^{Ph})_2(CH_3CN)](BF_4)_2$ in acetonitrile/0.2 M Et_4NBF_4 with a 1 mm glassy carbon working electrode; scans taken in the absence of (black) and in the presence of various concentrations of water and acid ($[(DMF)H]^+OTf$). Scan rate = 0.1 V s^{-1}.

rate for this complex is <1 s^{-1} under the same conditions where $[Ni(P^{n\text{-}Bu}{}_2N^{Ph}{}_2)_2(CH_3CN)]^{2+}$ has a catalytic rate of 46 s^{-1}, at least 1 order of magnitude faster.

The slow catalytic rate observed for $[Ni(P^{TP}{}_2N^{Ph}{}_2)_2(CH_3CN)]^{2+}$ provided an opportunity to assess the effect of water on the catalytic rate. Addition of water (2.5 M) to an acetonitrile solution of $[Ni(P^{TP}{}_2N^{Ph}{}_2)_2(CH_3CN)]^{2+}$ containing approximately 0.12 M [(DMF)H]OTf results in relatively large increases in current, as shown in Figure 9. The performance of this catalyst is enhanced from a rate less than 1 s^{-1} to a rate of 69 s^{-1}. Similar enhancements of the catalytic rates by 20−100 times are observed for all of the $[Ni(P^{R}{}_2N^{Ph}{}_2)_2(CH_3CN)]^{2+}$ catalysts with alkyl substituents on phosphorus, as shown in Table 6.

Previous studies have demonstrated that the nature of the acid plays an important role in determining the turnover frequencies for H_2 production using $[Ni(P^{Ph}{}_2N^{R}{}_2)_2(CH_3CN)]^{2+}$ complexes as electrocatalysts.[8] Similar effects were observed for the present series of complexes, and data shown in Table 6 indicate that the rates of catalysis decrease by up to an order of magnitude when bulkier anilinium acids are used in place of [(DMF)H]OTf.

DISCUSSION

On the basis of experimental[6,8] and theoretical[22] mechanistic studies of both hydrogen production and oxidation catalysts of the

Scheme 4. Proposed Catalytic Cycle for Hydrogen Production by $[Ni(P^{R}{}_2N^{Ph}{}_2)_2]^{2+}$ Catalysts[a]

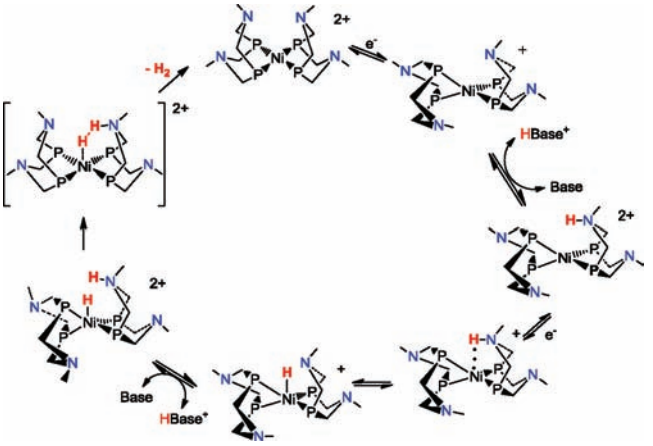

[a] Phosphine substituents not shown and N-substituents simplified for clarity.

type $[Ni(P^{R}{}_2N^{R'}{}_2)_2(CH_3CN)]^{2+}$, it has been proposed that the intermediate shown by structure **1** is required for the formation of the H−H bond during H_2 production.

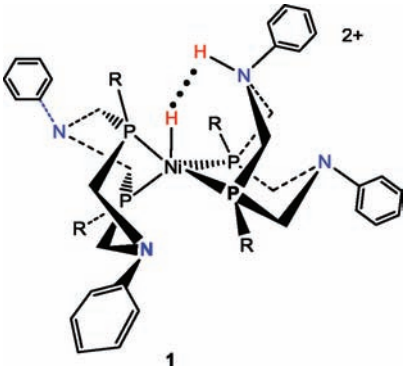

For such an intermediate, the driving force and rate of H_2 elimination should increase as the acidity of the protonated pendant amine increases and as the hydride donor ability of the metal increases. The proposed catalytic cycle is shown in Scheme 4. This cycle is consistent with the electrochemical observations discussed above, as well as previously studied $[Ni(P^{R}{}_2N^{Ph}{}_2)_2]^{2+}$ electrocatalysts for H_2 production.[4−8] The mechanism in Scheme 4 shows only endo protonation of the amines, leading to the formation of H_2. Scheme 5, discussed later, considers the results of exo protonation, pathways that do not lead directly to the production of H_2.

We recently reported a series of essentially isostructural $[Ni(P^{Ph}{}_2N^{C6H4X}{}_2)_2](BF_4)_2$ derivatives having pendant amines with a wide range of Brønsted basicities, obtained by varying the electron-donating character of X in the *N*-aryl *para* position. In general, the catalysts having more acidic protonated pendant amines experienced a larger driving force for H_2 elimination from intermediates with structure **1**, and a good correlation was observed between this driving force and the turnover frequencies for hydrogen formation.

Effect of Hydride Donor Ability on Catalytic Rates. The present study was designed to examine how variation in the substituent on phosphorus within a series of $[Ni(P^{R}{}_2N^{Ph}{}_2)_2(CH_3CN)]^{2+}$ complexes contributes to the observed catalytic rates

for H_2 formation. Previous studies have shown that the hydride donor abilities of $[HNi(diphosphine)_2]^+$ derivatives, as well as the Ni(II/I) couple of the corresponding $[Ni(diphosphine)_2]^{2+}$ complexes, are strongly influenced both by the electron-donating ability of substituents on the phosphorus atoms and by steric interaction between the two diphosphine ligands.[16,18,23] The previously documented trend that sterically more demanding substituents on phosphorus lead to more positive $E_{1/2}$ values for the Ni(II/I) redox couple and to weaker hydride donor abilities (larger $\Delta G°_{H-}$ values) has been attributed to a larger dihedral angle between the two planes defined by the phosphorus atoms of each diphosphine ligand and Ni in $[Ni(diphsophine)_2]^{2+}$ complexes. This tetrahedral distortion leads to lower LUMO energies as a result of a decrease in the antibonding overlap of the σ orbitals of phosphorus with the d_{xy} orbital of nickel.[23] In the previously studied $[Ni(P^{Ph}{}_2N^{C6H4X}{}_2)_2]^{2+}$ systems, in which the acidities of the protonated amines were varied, all P atoms were substituted with phenyl groups and very little structural variation between catalysts was expected. For the series of $[Ni(P^R{}_2N^{Ph}{}_2)_2(CH_3CN)]^{2+}$ derivatives studied in this work, all of the pendant amines have a Ph substituent, so it is assumed that the basicity of the proton relay will not vary significantly. Changes in driving force for H_2 production should be derived primarily from changes in hydride donor ability associated with different substituents on the phosphorus donors of the ligands.

The data shown in Table 5 and Figure 5 show that the hydride donor abilities determined for $[HNi(P^R{}_2N^{Ph}{}_2)_2]^+$ derivatives and the resulting driving force for H_2 elimination differ by approximately 7 kcal/mol upon varying the alkyl substituent R from cyclohexyl to *n*-butyl. In studies using [(DMF)H]OTf as the acid, the complexes with $\Delta G°_{H2}$ values most favorable for H_2 elimination, $[Ni(P^{n\text{-}Bu}{}_2N^{Ph}{}_2)_2(CH_3CN)]^{2+}$ and $[Ni(P^{PE}{}_2N^{Ph}{}_2)_2(CH_3CN)]^{2+}$, display the highest turnover frequencies for H_2 production in this series. However, other data in Tables 5 and 6 indicate that in some cases the catalytic rate of H_2 production does not parallel the driving force for H_2 elimination. For example, the largest *difference* in turnover frequencies is observed for $[Ni(P^{n\text{-}Bu}{}_2N^{Ph}{}_2)_2(CH_3CN)]^{2+}$ and $[Ni(P^{TP}{}_2N^{Ph}{}_2)_2(CH_3CN)]^{2+}$, while the estimated driving force for H_2 elimination differs by only 0.5 kcal/mol, which is essentially the same within our experimental uncertainty. In contrast, the turnover frequencies for both $[Ni(P^{Bn}{}_2N^{Ph}{}_2)_2(CH_3CN)]^{2+}$ and $[Ni(P^{TP}{}_2N^{Ph}{}_2)_2(CH_3CN)]^{2+}$ are similarly low for all conditions studied, despite their comparatively large difference in $\Delta G°_{H2}$ (1.8 kcal/mol). Unfortunately, the derivative with R = cyclohexyl is unstable in the acidic solutions required for catalysis of H_2 production, so it could not be included in these comparisons. The lack of correlation between the catalytic rates and the corresponding $\Delta G°_{H2}$ values for some of the complexes suggests that factors other than the thermodynamics of H−H bond formation can play an important role in determining the catalytic activities.

Although the potentials of the Ni(II/I) couples are sensitive to both electronic effects and interactions between the phosphine substituents, the potentials of the Ni(I/0) couples for the $[Ni(diphosphine)_2]^{2+}$ complexes are determined almost exclusively by the electronic character of the phosphorus substituent;[16] $[Pd(diphosphine)_2{}^{2+}]$ complexes exhibit similar trends.[24] Therefore, a second way of evaluating the influence of steric effects between diphosphines in this series of complexes is to consider the difference in the potentials of the Ni(II/I) and Ni(I/0) couples ($\Delta E_{1/2}$). These $\Delta E_{1/2}$ values are listed in Table 4, and they fall into three groups. The largest steric interaction between substituents

Scheme 5. Protonation of Pendant Amines Endo or Exo with Respect to Nickel

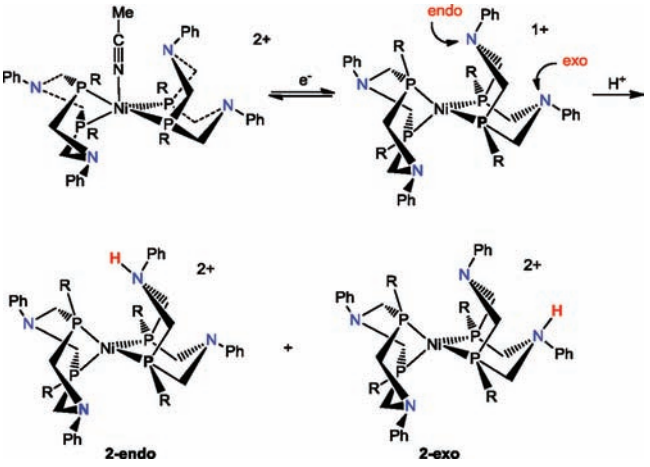

on phosphorus is observed for the cyclohexyl substituted complex, $[Ni(P^{Cy}{}_2N^{Ph}{}_2)_2(CH_3CN)]^{2+}$ ($\Delta E_{1/2}$ = 0.52 V); the smallest steric interaction is observed for the phenyl substituted complex, $[Ni(P^{Ph}{}_2N^{Ph}{}_2)_2]^{2+}$ ($\Delta E_{1/2}$ = 0.18 V); and the complexes $[Ni(P^{n\text{-}Bu}{}_2N^{Ph}{}_2)_2(CH_3CN)]^{2+}$, $[Ni(P^{Bn}{}_2N^{Ph}{}_2)_2(CH_3CN)]^{2+}$, $[Ni(P^{TP}{}_2N^{Ph}{}_2)_2(CH_3CN)]^{2+}$, and $[Ni(P^{PE}{}_2N^{Ph}{}_2)_2(CH_3CN)]^{2+}$ exhibit $\Delta E_{1/2}$ values between 0.26 and 0.30 V. Despite the similar degree of steric interaction between alkyl substituents of adjacent phosphine ligands in the last group, large differences in turnover frequencies are observed for this series, as described above.

Effect of Additional Steric Interactions. A consideration of the mechanistic steps proposed[4] for the production of H_2 by these catalysts suggests how additional steric interactions of the phosphine substituents may be an important factor in determining the catalytic rate. The cyclic voltammograms shown in Figures 6 and 8 indicate that the reduction of Ni(II) to Ni(I) is followed by a fast protonation reaction, and this proton addition is proposed to occur at a pendant amine of the ligand, which serves as a proton relay. This protonation may occur in either endo or exo positions with respect to nickel as shown by structures **2-endo** and **2-exo** in Scheme 5.

Fast protonation in either position would result in the observed positive shift in the reduction potential. However, in order for the complex to enter the catalytic cycle, the site of protonation of the Ni(I) intermediate must be endo with respect to the Ni atom. In conjunction with the second electron transfer, the second protonation must also occur in an endo position in order to form intermediate **1**.

As discussed above, the first protonation of the catalyst occurs in the Ni(I) oxidation state. Because both $[Ni^I(diphosphine)_2]^+$ and $Ni^0(diphosphine)_2$ complexes exhibit distorted tetrahedral structures, the structure of $Ni^0(P^{Bn}{}_2N^{Ph}{}_2)_2$ (Figure 3) is of special interest. The structure indicates that the region near the metal center is shielded by considerable steric bulk and suggests that the most likely site of protonation for this complex is the exo position. Previous NMR studies of the closely related $Ni^0(P^{Ph}{}_2N^{Bn}{}_2)_2$ complex demonstrated that protonation by 2,6-dichloroanilinium tetrafluoroborate in the exo postions is preferred.[9] It is also apparent from the structure of $Ni^0(P^{Bn}{}_2N^{Ph}{}_2)_2$ that the positions of the phosphine substituents can give rise to unfavorable steric interactions with the amine group of the opposing $P^{Bn}{}_2N^{Ph}{}_2$ ligand, and have the potential to hinder endo protonation of the

dx.doi.org/10.1021/ic201461a |*Inorg. Chem.* 2011, 50, 10908–10918

amines. This steric interaction corresponds with our observations that alkyl groups have a more pronounced effect on the catalytic rates than phenyl substituents, and that larger alkyl substituents on phosphorus result in slower catalytic rates. In particular, it appears that alkyl substituents with groups attached at a distance of two or more atoms from the phosphorus atom are effective at retarding the rate of catalysis by blocking access of acid to the endo positions of the N atoms. For example, the 2,4,4-trimethylpentyl substituent does not manifest its steric bulk by resulting in significant interactions between phosphines in adjacent ligands in the Ni(II) oxidation state (as indicated by a $\Delta E_{1/2}$ of 0.28 V for $[Ni(P^{TP}{}_2N^{Ph}{}_2)_2(CH_3CN)]^{2+}$ compared to the $\Delta E_{1/2}$ of 0.30 V for $[Ni(P^{n\text{-}Bu}{}_2N^{Ph}{}_2)_2(CH_3CN)]^{2+}$). However, the very low catalytic rate for this complex can be understood in terms of the distal bulk of the 2,4,4-trimethylpentyl substituent preventing the formation of significant amounts of the endo protonated intermediates necessary for catalysis.

Previous work with the $[Ni(P^{Ph}{}_2N^{C6H4X}{}_2)_2]^{2+}$ catalysts has demonstrated that water enhanced the rate of hydrogen production.[8] For example, addition of water (0.02−0.5 M) to reaction mixtures containing 0.20−0.45 M [(DMF)H]OTf increased the catalytic rates by 30−60%. In addition, the rates of catalysis with this series of complexes were dependent on the nature of the acid substrate. Both cyanoanilinium ($pK_a^{MeCN} = 7.0$) and 2,6 dichloroanilinium ($pK_a^{MeCN} = 5.0$) were found to be about an order of magnitude slower than those observed for [(DMF)H]OTf ($pK_a^{MeCN} = 6.1$), although their pK_a values bracketed that of [(DMF)H]OTf.[25]

Similar effects were observed for the present series of complexes, and these are also attributed to the steric limitations to endo protonation imposed by bulky phosphine substituents. In this series of complexes the smaller acid [(DMF)H]OTf gave faster catalytic rates than those observed for the larger cyanoanilinium acid by as much as an order of magnitude. Similarly, water is likely to assist in the delivery of protons to the endo position of these catalysts, being smaller than either [(DMF)H]OTf or cyanoanilinium, but capable of hydrogen bonding to serve as a relay to the pendant base. The observation that water enhances the catalytic rates for H_2 production more for the $[Ni(P^R{}_2N^{Ph}{}_2)_2(CH_3CN)](BF_4)_2$ catalysts reported in this study (by factors of 10 to >70, Table 6) than observed previously for $[Ni(P^{Ph}{}_2N^{C6H4X}{}_2)_2](BF_4)_2$ catalysts (30−60%) is attributed to the greater steric bulk of the alkyl substituents on phosphorus compared to the phenyl substituent in the latter series. The more sterically demanding alkyl substituents present a more restricted access for endo protonation, and the preferential access by small water molecules acting as intermolecular proton relays to the pendant amines should lead to a larger enhancement of the catalytic rate.

SUMMARY AND CONCLUSIONS

In the catalytic production of H_2 with $[Ni(P^R{}_2N^{Ph}{}_2)_2(CH_3CN)]^{2+}$ derivatives, the rate of H_2 elimination from the proposed intermediate of structure **1** should be favored by increased acidities of the protonated amines and by stronger hydride donor abilities of the metal center.

In order to determine the effect of hydride donor ability on the rates of electrocatalytic proton reduction, a series of complexes of the formula $[Ni(P^R{}_2N^{Ph}{}_2)_2(CH_3CN)]^{2+}$ containing different alkyl groups at the phosphorus atoms of the $P^R{}_2N^{Ph}{}_2$ ligands were synthesized and characterized. Both electronic properties of phosphine substituents and steric interactions between adjacent phosphine ligands have been shown to influence the hydride donor ability of $[HNi(P^R{}_2N^{Ph}{}_2)_2]^+$ derivatives. For some cases in this series of catalysts, the turnover frequencies for H_2 formation were found to correlate with $\Delta G^\circ_{H^-}$ and consequently ΔG°_{H2}, but for several of the complexes, catalytic rates do not follow the trend predicted on the basis of these properties (Figure 10).

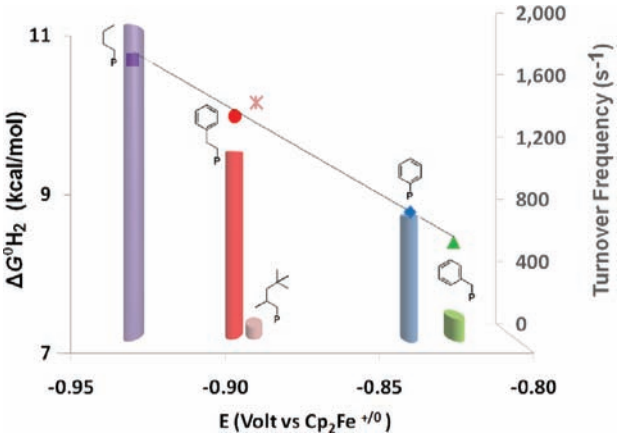

Figure 10. Plot of ΔG°_{H2} as a function of $E_{1/2}$ of the Ni(II/I) couple, superimposed on a bar graph of turnover frequencies.

The catalytic reaction proceeds through protonation of pendant amines in tetrahedral Ni(I) and Ni(0) intermediates, and the turnover frequencies appear to be sensitive to the extent that the steric bulk of the phosphine substituent hinders the endo protonation of the amine of the adjacent ligand in these intermediates. The addition of water to these systems leads to a significant increase in catalytic rates, and this effect is attributed to the ability of water to assist in the generation of catalytically active intermediates that are protonated endo relative to nickel. These studies suggest that structural modifications of the complexes that enable the delivery of protons to endo sites should further increase the turnover frequencies of these catalysts; studies to achieve this goal are currently in progress.

EXPERIMENTAL SECTION

General Experimental Procedures. *Instrumentation.* ^1H and ^{31}P NMR spectra were recorded on Varian spectrometers (Inova or VNMRS, 500 MHz for ^1H) at 23 °C unless otherwise noted. All ^1H chemical shifts have been internally calibrated to the residual solvent protons. ^{31}P NMR spectra were externally referenced to H_3PO_4 at 0 ppm. Electrospray ionization (ESI), chemical ionization (CI), and atmospheric pressure chemical ionization (APCI) mass spectra were collected at the Indiana University Mass Spectrometry Facility on a Waters/Micromass LCT Classic (ESI/APCI) or Thermo MAT-95 XP (EI/CI) using anhydrous solvents and inert atmosphere techniques.

Electrochemistry. Unless otherwise indicated in the text, voltammetric procedures were conducted in 0.2 M NEt_4BF_4/CH_3CN at ambient temperature, 23 °C, under nitrogen using a Vacuum Atmospheres glovebox. A standard three-electrode configuration was employed in conjunction with CH Instruments 660C or 1100C potentiostat interfaced to a computer with CH Instruments 700 D software. All voltammetric scans were recorded using glassy-carbon working electrode disks of 1 mm diameter encased in PEEK (Cypress Systems EE040). The working electrode was treated between scans by polishing with diamond paste (Buehler) in sequence of decreasing sizes (3−0.25 μm) interspersed by washings with purified H_2O (*vide infra*). A glassy-carbon rod (Structure Probe, Inc.) and platinum wire (Alfa-Aesar) were used as auxiliary electrodes

and quasireference electrodes respectively. All glassware for electrochemical experiments was oven-dried overnight and allowed to cool under vacuum. Ferrocene was used as an internal standard, and all potentials reported within this work are referenced to the ferrocenium/ferrocene couple at 0 V.

Synthesis and Materials. All reactions and manipulations were performed under an N_2 atmosphere using standard Schlenk techniques or in a glovebox unless otherwise indicated. Solvents were dried using an Innovative Technology, Inc. PureSolv solvent purification system. Acetonitrile-d_3 (Cambridge Isotope Laboratories, 99.5%D) was vacuum-distilled from P_2O_5. Chloroform-*d* (Cambridge Isotope Laboratories, 99.5%D) was degassed and stored over molecular sieves. Tetraethylammonium tetrafluoroborate (Alfa-Aesar) was recrystallized twice by vapor diffusion of diethyl ether into an acetonitrile solution; the crystals obtained were dried under vacuum. Dimethylformamide-trifluoromethanesulfonic acid, $[(DMF)H]^+OTf^-$, was prepared by the method of Faviera and Duñach.[19] 2,4,4-Trimethylpentylphosphine (Strem) was used as received. Water was dispensed from a Millipore Milli-Q purifier and sparged with nitrogen. Ferrocene (Aldrich) was sublimed under vacuum before use. $[Ni(CH_3CN)_6](BF_4)_2\cdot 1/2CH_3CN$,[26] $[Ni(P_2^{Cy}N_2^{Ph})_2(CH_3CN)](BF_4)_2$,[15] $P_2^{Cy}N_2^{Ph}$,[27] *n*-butylphosphine,[28] benzylphosphine,[28] and 2-phenylethylphosphine[28] were prepared by the literature methods.

Synthesis of $P^{Bn}{}_2N^{Ph}{}_2$. A 250 mL Schlenk flask was charged with benzylphosphine (2.8 g, 23 mmol), paraformaldehyde (1.4 g, 47 mmol), and ~100 mL of degassed absolute ethanol. The resulting suspension was immersed in a hot oil bath (70 °C) and stirred for 12 h, resulting in a clear solution. The $^{31}P\{^1H\}$ NMR spectrum of the crude reaction mixture exhibited a singlet at −14 ppm which is assigned to bis(hydroxymethyl)benzylphosphine. A degassed solution of aniline (2.1 g, 23 mmol) in 10 mL of ethanol was added dropwise to the hot solution of bis(hydroxymethyl)benzylphosphine over a period of 2 h. The resulting suspension of a white precipitate was heated for an additional 4 h at 70 °C and was further heated at 50 °C overnight. The solvent was removed on a vacuum line, and the resulting product was suspended in Et_2O and stirred for 1 h. The white solid was collected by filtration and dried in vacuo (yield 2.8 g, 5.8 mmol, 52%). $^{31}P\{^1H\}$ NMR ($CDCl_3$, 202.3 MHz): δ −46.0 (s). ^1H NMR ($CDCl_3$, 499.7 MHz): δ 7.33 (m, 10H, Ar*H*); 6.99 (m, 4H, Ar*H*); 6.59 (m, 2H, Ar*H*); 6.16 (m, 4H, Ar*H*); 4.21 (dd, J = 14.8 Hz, 3.8 Hz, 4H, PCH_2N); 3.45 (dd, J = 14.8 Hz, 10.1 Hz, 4H, PCH_2N); 2.83 (d, J = 2.8 Hz, 4H, PCH_2Ar). CI-MS: Observed MH^+ at 483.2118. Calculated for MH^+: 483.2113. Anal. Calcd for $C_{30}H_{32}N_2P_2$: C, 74.67; H, 6.68; N, 5.81. Found C, 74.67; H, 6.66; N, 5.86.

Synthesis of $P^{n\text{-}Bu}{}_2N^{Ph}{}_2$. A 250 mL Schlenk flask was charged with *n*-butylphosphine (2.2 g, 24 mmol), paraformaldehyde (5 g, 167 mmol), and ~100 mL of degassed absolute ethanol. The resulting suspension was immersed in an oil bath (45 °C) and stirred for 12 h, resulting in a clear solution. A singlet in the ^{31}P NMR spectrum suggests formation of the bis(hydroxymethyl)butylphosphine (−22 ppm; EtOH). Aniline (1.6 g, 17 mmol) in toluene (~2 mL) was added dropwise over 2 h to the hot solution. The resulting white suspension was heated for 4 h at 70 °C and was further heated at 50 °C overnight. The solvent was then removed on a vacuum line, and the product was suspended and stirred in diethyl ether. The suspension was filtered, and the white solid was dried in vacuo (yield 1.6 g, 3.9 mmol, 45% based on aniline). $^{31}P\{^1H\}$ NMR ($CDCl_3$, 202.2 MHz): δ −50.0 (s). ^1H NMR ($CDCl_3$, 499.7 MHz): δ 7.20 (t, J = 6.5 Hz, 4H, Ar*H*); 6.69 (d, J = 8.1 Hz, 6H, Ar*H*); 4.20 (m, 4H, PCH_2N); 3.44 (m, 4H, PCH_2N); 1.61 (m, 4H, CH_2); 1.49 (m, 4H, CH_2); 1.41 (m, 4H, CH_2); 0.98 (m, 6H, CH_3). CI-MS: Observed MH^+ at 415.2408. Calculated for MH^+: 415.2426.

Synthesis of $P^{PE}{}_2N^{Ph}{}_2$. A 250 mL Schlenk flask was charged with 2-phenylethylphosphine (2.0 g, 14 mmol) dissolved in ~80 mL of THF. To this solution was added paraformaldehyde (1.6 g, 53 mmol) suspended in degassed absolute ethanol. The flask was immersed in an oil bath (70 °C) and stirred for two days. A singlet at −24 ppm in the ^{31}P NMR spectrum of the crude reaction mixture was consistent with formation of the bis(hydroxymethyl)-2-phenylethylphosphine. To the reaction mixture was added degassed aniline (500 mg, 5.37 mmol) portionwise to the hot solution over a period of 4 h. The resulting suspension of white precipitate was heated for 8 h at 70 °C. The volume of the reaction mixture was reduced under vacuum, and a white solid was collected by filtration (yield 420 mg, 0.823 mmol, 30% based on aniline). $^{31}P\{^1H\}$ NMR ($CDCl_3$, 202.2 MHz): δ −49.0 (s). ^1H NMR ($CDCl_3$, 499.7 MHz): δ 7.33 (t, J = 7.6 Hz, 4H, Ar*H*); 7.26 (m, 4H, Ar*H*); 7.23 (m, 2H, Ar*H*); 7.18 (t, J = 7.7 Hz, 4H, Ar*H*); 6.68 (td, J = 7.3 Hz, 7.3 Hz, 0.8 Hz, 2H, Ar*H*); 6.59 (d, J = 8.7, 4H, Ar*H*); 4.13 (t, J = 14.5 Hz, 4H, CH_2); 3.44 (dd, J = 15.0 Hz, 4.4 Hz, 4H, CH_2); 2.95 (dd, J = 16.4 Hz, 8.3 Hz, 4H, CH_2); 1.72 (m, 4H, CH_2). CI-MS: Observed MH^+ at 511.2450. Calculated for MH^+: 511.2432.

Synthesis of $P^{TP}{}_2N^{Ph}{}_2$. A 100 mL Schlenk flask was charged with 2,4,4-trimethylpentylphosphine (4.8 g, 33 mmol mmol), paraformaldehyde (2.0 g, 67 mmol), and ~20 mL of degassed absolute ethanol. The resulting suspension was immersed in a hot oil bath (75 °C) and stirred for 12 h, resulting in a clear solution. A ^{31}P NMR spectrum recorded on the reaction mixture at this point was consistent with formation of the bis(hydroxymethyl)-2,4,4-trimethylpentylphosphine (−27 ppm, s; EtOH) which was isolated as a clear, highly viscous oil by removal of all volatiles in vacuo (6.2 g, 30 mmol, 94%). To a 100 mL Schlenk flask was added 1.0 g (4.8 mmol) of bis(hydroxymethyl)-2,4,4-trimethylpentylphosphine and 30 mL of ethanol. To this solution was added a degassed toluene solution (~2 mL) of aniline (450 mg, 4.8 mmol) over a period of 2 h. After 3 h of stirring at 65 °C a white suspension was observed. The reaction mixture was heated at 50 °C overnight. The solid was collected by filtration, washed with diethyl ether, and dried in vacuo (yield 747 mg, 1.4 mmol, 58%). $^{31}P\{^1H\}$ NMR ($CDCl_3$, 202.2 MHz): δ −53.0 (s). Anal. Calcd for $C_{32}H_{52}N_2P_2$: C, 72.97; H, 9.95; N, 5.32. Found C, 73.18; H, 10.08; N, 5.29. APCI-MS: Observed MH^+ at 527.3668. Calculated for MH^+: 527.3684.

Synthesis of $[Ni(P^{Bn}{}_2N^{Ph}{}_2)_2(CH_3CN)](BF_4)_2$. To a stirred MeCN solution (15 mL) of $[Ni(CH_3CN)_6](BF_4)_2\cdot 1/2CH_3CN$ (101 mg, 0.202 mmol) was added 2 equiv of $P^{Bn}{}_2N^{Ph}{}_2$ (200 mg, 0.415 mmol). The blue solution of $[Ni(CH_3CN)_6](BF_4)_2\cdot 1/2CH_3CN$ rapidly changed to a red color. The resultant red solution was filtered through a plug of Celite after stirring overnight. The remaining solvent was removed from the filtrate under vacuum. The red powder was washed with diethyl ether and dried *in vacuo* (yield 215 mg, 174 mmol, 86%). $^{31}P\{^1H\}$ NMR (CD_3CN, 202.2 MHz): δ 5.2 (s). ^1H NMR (CD_3CN, 499.7 MHz): δ 7.40 (m, 12H, Ar*H*); 7.33 (m, 8H, Ar*H*); 7.16 (m, 8H, Ar*H*); 7.04 (t, J = 7.3 Hz, 4H, Ar*H*); 6.86 (d, J = 7.9 Hz, 8H, Ar*H*); 3.99 (d, J = 14.1 Hz, 8H, PCH_2N); 3.70 (s, 8H, PCH_2Ar); 3.44 (d, J = 14.0 Hz, 8H, PCH_2N) 1.96 (s, 3H, CH_3CN). MS-ESI: Observed $\{[Ni(P^{Bn}{}_2N^{Ph}{}_2)_2](BF_4)\}^+$ 1109.3481. Calculated for $\{[Ni(P^{Bn}{}_2N^{Ph}{}_2)_2](BF_4)\}^+$: 1109.3464.

Synthesis of $[Ni(P^{n\text{-}Bu}{}_2N^{Ph}{}_2)_2(CH_3CN)](BF_4)_2$. This complex was prepared in a manner analogous to that described for $[Ni(P^{Bn}{}_2N^{Ph}{}_2)_2(CH_3CN)](BF_4)_2$. The product was isolated as a red powder in 91% yield. The complex may be further purified by slow diffusion of hexanes into a THF solution of the complex, resulting in red powder. $^{31}P\{^1H\}$ NMR (CD_3CN, 202.2 MHz): δ 7.8 (s). ^1H NMR (CD_3CN, 499.7 MHz): δ 7.39 (m, 8H, Ar*H*); 7.08 (d, J = 7.3 Hz, 8H, Ar*H*); 7.02 (t, 4H, Ar*H*); 6.85 (m, 4H, Ar*H*); 3.83 (m, 8H, PCH_2N); 3.68 (m, 8H, PCH_2N); 2.16 (m, 8H, CH_2); 1.96 (s, 3H, CH_3CN); 1.57 (m, 8H, CH_2); 1.46 (m, 8H, CH_2); 0.92 (t, 12H, CH_3). ESI-MS: Observed $\{[Ni(P_2N_2)_2](BF_4)\}^+$ 973.4071. Calculated for $\{[Ni(P_2N_2)_2](BF_4)\}^+$: 973.4090.

Synthesis of $[(Ni(P^{TP}{}_2N^{Ph}{}_2)_2(CH_3CN)](BF_4)_2$. This complex was prepared in a manner analogous to that described for $[Ni(P^{Bn}{}_2N^{Ph}{}_2)_2(CH_3CN)](BF_4)_2$. The product was isolated as a red powder in 76% yield. $^{31}P\{^1H\}$ NMR (CD_3CN, 202.2 MHz): δ 8.5 (s). ^1H NMR (CD_3CN,

499.7 MHz): δ 7.36 (m, 8H, ArH); 7.09 (m, 12H, ArH); 3.87 (m, 8H, PCH$_2$N); 3.77 (m, 8H, PCH$_2$N); 2.17 (m, 8H, CH$_2$); 2.02 (m, 4H, CH); 1.96 (s, 3H CH$_3$CN); 1.35 (m, 8H, CH$_2$); 1.13 (m, 12H, CH$_3$); 0.89 (s, 36H, CH$_3$). ESI-MS: Observed $\{[Ni(P_2N_2)_2](BF_4)\}^+$ 1197.6565. Calculated for $\{[Ni(P_2N_2)_2](BF_4)\}^+$: 1197.6594.

Synthesis of $[(Ni(P^{PE}{}_2N^{Ph}{}_2)_2(CH_3CN)](BF_4)_2$. This complex was prepared in a manner analogous to that described for $[Ni(P^{Bn}{}_2N^{Ph}{}_2)_2(CH_3CN)](BF_4)_2$. The product was isolated as a red powder in 91% yield. $^{31}P\{^1H\}$ NMR (CD_3CN, 202.2 MHz): δ 6.8 (s). ^1H NMR (CD_3CN, 499.7 MHz): δ 7.32 (m, 14H, ArH); 7.28 (m, 6H, ArH); 7.15 (m, 8H, ArH); 7.06 (t, J = 7.4 Hz, 4H, ArH); 6.98 (d, J = 7.9 Hz, 8H, ArH); 3.84 (m, 8H, PCH$_2$N); 3.71 (m, 8H, PCH$_2$N); 2.98 (m, 8H, CH$_2$); 2.50 (m, 8H, CH$_2$); 1.96 (s, 3H, CH$_3$CN). Anal. Calcd for $C_{66}H_{75}B_2F_8N_5NiP_4$: C, 61.23; H, 5.84; N, 5.41. Found C, 61.01; H, 6.07; N, 5.67. ESI-MS: Observed $\{[Ni(P_2N_2)_2](BF_4)\}^+$ at 1165.4124. Calculated for $\{[Ni(P_2N_2)_2](BF_4)\}^+$: 1165.4090.

Synthesis of $Ni(P^{Bn}{}_2N^{Ph}{}_2)_2$. To a stirred MeCN solution (7 mL) of $[Ni(CH_3CN)_6](BF_4)_2 \cdot 1/2CH_3CN$ (52 mg, 0.10 mmol) was added 2 equiv of $P^{Bn}{}_2N^{Ph}{}_2$ (100 mg, 0.207 mmol). The blue solution of $[Ni(CH_3CN)_6](BF_4)_2 \cdot 1/2CH_3CN$ rapidly changed to a red color. The solution was stirred for 4 h at room temperature; then, tetramethylguanidine (40 mg, 35 mmol) was added. A white precipitate presumed to be P_2N_2 ligand was observed. The mixture was then bubbled with H_2 gas for 10 min, followed by stirring for 2 days. The resulting mixture was filtered, concentrated, and stored. After sitting for four days at room temperature under N_2, yellow crystals were observed and collected (yield 25 mg, 0.024 mmol, 24%). $^{31}P\{^1H\}$ NMR (C_6D_6, 202.2 MHz): δ −1.03 (s). ^1H NMR (C_6D_6, 499.7 MHz): δ δ 7.19 (m, 8H, ArH); 7.16 (m, 16H, ArH); 7.08 (m, 4H, ArH); 6.78 (m, 8H, ArH); 6.74 (d, 4H, ArH); 3.34 (m, 16H, PCH$_2$N); 2.70(s, 8H, PCH$_2$Ar). Anal. Calcd for $C_{60}H_{64}N_4NiP_4$: C, 70.39; H, 6.30; N, 5.47. Found: C, 70.48; H, 6.37; N, 5.54.

Equilibration of $[Ni(P^R{}_2N^{Ph}{}_2)_2(CH_3CN)](BF_4)_2$ with H_2 and Anisidine/Anisidinium or Bromoaniline/Bromoanilinium in Acetonitrile-d_3. In a typical experiment, $[Ni(P^R{}_2N^{Ph}{}_2)_2(CH_3CN)](BF_4)$ and *p*-bromoaniline (pK_a = 9.43) or *p*-anisidine (pK_a = 11.83) were accurately weighed into an NMR tube and dissolved in acetonitrile-d_3 (0.5 mL). Hydrogen gas was bubbled through the solution for 10 min. The solution was allowed to sit for 15 min and was monitored by ^1H NMR and ^{31}P NMR spectroscopy. The reaction came to equilibrium within the time of mixing and was monitored every few hours for 24 h to ensure that the ratios had not changed. The ^1H and ^{31}P NMR resonances assigned to $[Ni(P^R{}_2N^{Ph}{}_2)_2(CH_3CN)](BF_4)_2$ and the corresponding hydrides, $[HNi(P^R{}_2N^{Ph}{}_2)_2](BF_4)$, were integrated, and the ratio was used to determine the equilibrium constant for the reaction. The ratio of $[Hbase^+]/[base]$ was determined from the observed ^1H NMR chemical shift. Three separate experiments were run to determine the reproducibility. The equilibrium constant ($K = [NiH^+][Hbase^+]/P_{H2}[Ni^{2+}][base]$) was used to calculate the hydride donor ability. Values of $\Delta G°_{H-}$ are reported as an average of three runs. The standard deviation for values reported is less than 0.5 kcal/mol. Purging the samples with N_2 gas for 15 min resulted in the observation of only $[Ni(P^R{}_2N^{Ph}{}_2)_2(CH_3CN)](BF_4)_2$.

Catalytic Hydrogen Production Using $[Ni(P^{n\text{-}Bu}{}_2N^{Ph}{}_2)_2(CH_3CN)](BF_4)_2$ as Catalyst and [(DMF)H]OTf as Acid. Typical Experimental Conditions. $[Ni(P^{n\text{-}Bu}{}_2N^{Ph}{}_2)_2(CH_3CN)](BF_4)_2$ (2.1 mg, 0.002 mmol) and ferrocene (0.4 mg, 0.002 mmol) were weighed into an 8 mL glass vial and dissolved in 2 mL of a supporting electrolyte solution (0.2 M $[NEt_4][BF_4]$/acetonitrile). Purity of the electrolyte medium was confirmed over the available electrochemical window through background scans taken prior to addition of analyte. In a separate vial, 100 mg (0.45 mmol) of [(DMF)H]OTf was dissolved in 0.6 mL of acetonitrile. Acidic titrant was transferred to the electrochemical solution via volumetric syringe in 20 μL aliquots. Subsequent to each addition of titrant, the working electrode was cleaned by polishing (*vide supra*), and a cyclic voltammogram was recorded. The catalytic current (i_{cat}) was selected in each instance at the most positive potential beyond the Ni(II/I) $E_{1/2}$ at which current stopped increasing. Addition of acidic titrant was continued until catalytic current enhancement ceased (ca. 0.12 M [(DMF)H]OTf). Subsequent to the completion of acid additions, the described method was repeated using aliquots of purified H_2O as titrant. H_2O was added by Eppendorf automatic micropipeter in 3−10 μL increments until the observed catalytic current enhancement ceased or catalytic current was reduced.

Catalytic Hydrogen Production. Controlled Potential Coulometry. A three-necked flask having a total volume of 150 mL was used as the bulk electrolysis vessel, and was assembled under an atmosphere of nitrogen with each neck accepting an electrode fed through a pierced rubber septum. The working electrode consisted of a copper wire attached to a reticulated vitreous carbon cylinder; the reference and counter electrodes were a Ag wire and graphite rod, respectively, placed into 5 mm glass tubes terminating in Vycor fritted disks and filled via syringe with electrolyte solution (0.3 M Et_4NBF_4 in acetonitrile). A solution of $[Ni(P^{PE}{}_2N^{Ph}{}_2)_2(CH_3CN)](BF_4)_2$ (13 mg, 0.010 mmol), ferrocene, and NEt_4BF_4 (1.0 g, 4.6 mmol) in 10 mL of acetonitrile and a solution of [(DMF)H]OTf (670 mg, 3.0 mmol) in 5 mL of acetonitrile were prepared in the glovebox. The catalyst/ferrocene solution was then transferred to the reaction vessel via syringe, and a cyclic voltammogram was obtained. The acid solution was then added, and controlled-potential coulometry was performed at −1.0 V versus the ferricinium/ferrocene couple. After 17.5 C of charge was passed, a 200 μL sample of the headspace gas was removed via gastight syringe and analyzed by gas chromatography. Using the moles of H_2 produced and the charge passed, a current efficiency of 95 ± 5% was calculated for H_2 production (TON = 9, 25% decomposition). Gas analysis for H_2 was performed using an Agilent 6850 gas chromatograph equipped with a thermal conductivity detector and fitted with a 10 ft long Supelco 1/8″ Carbosieve 100/120 column, calibrated with two $H_2/N_2/CO/CO_2$ mixtures of known composition.

■ ASSOCIATED CONTENT

Ⓢ Supporting Information. CIF data for $[Ni(P^{Bn}{}_2N^{Ph}{}_2)_2(CH_3CN)]^{2+}$, $[Ni(P^{n\text{-}Bu}{}_2N^{Ph}{}_2)_2(CH_3CN)]^{2+}$, and $Ni(P^{Bn}{}_2N^{Ph}{}_2)_2$. Additional tabulated and graphical data for electrocatalytic hydrogen production. Cyclic voltammograms. This material is available free of charge via the Internet at http://pubs.acs.org.

■ AUTHOR INFORMATION

Corresponding Author

*E-mail: daniel.dubois@pnnl.gov (D.L.D.); morris.bullock@pnnl.gov (R.M.B.).

Notes

[‖] Sabbatical Visitor at PNNL, 2010−2011.

■ ACKNOWLEDGMENT

This research was supported as part of the Center for Molecular Electrocatalysis, an Energy Frontier Research Center funded by the U.S. Department of Energy, Office of Science under FWP 56073. Pacific Northwest National Laboratory is operated by Battelle for the U.S. Department of Energy.

■ REFERENCES

(1) (a) Lewis, N. S.; Nocera, D. G. *Proc. Natl. Acad. Sci. U.S.A.* **2006**, *103*, 15729–15735. (b) Cook, T. R.; Dogutan, D. K.; Reece, S. Y.; Surendranath, Y.; Teets, T. S.; Nocera, D. G. *Chem. Rev.* **2010**, *110*, 6474–6502.

(2) (a) Fontecilla-Camps, J. C.; Volbeda, A.; Cavazza, C.; Nicolet, Y. *Chem. Rev.* **2007**, *107*, 4273–4303. (b) Frey, M. *ChemBioChem* **2002**, *3*, 153–160.

(3) (a) Gloaguen, F.; Rauchfuss, T. B. *Chem. Soc. Rev.* **2009**, *38*, 100–108. (b) Tard, C.; Pickett, C. J. *Chem. Rev.* **2009**, *109*, 2245–2274. (c) Tard, C.; Liu, X.; Ibrahim, S. K.; Bruschi, M.; Gioia, L. D.; Davies, S.; Yang, X.; Wang, L.-S.; Sawers, G.; Pickett, C. J. *Nature* **2005**, *434*, 610–613. (d) Jiang, S.; Liu, J.; Shi, Y.; Wang, Z.; Åkermark, B.; Sun, L. *Dalton Trans* **2007**, 896–902. (e) Gloaguen, F.; Lawrence, J. D.; Schmidt, M.; Wilson, S. R.; Rauchfuss, T. B. *J. Am. Chem. Soc.* **2001**, *123*, 12518–12527. (f) van der Vlugt, J. I.; Rauchfuss, T. B.; Whaley, C. M.; Wilson, S. R. *J. Am. Chem. Soc.* **2005**, *127*, 16012–16013. (g) Barton, B. E.; Olsen, M. T.; Rauchfuss, T. B. *J. Am. Chem. Soc.* **2008**, *130*, 16834–16835. (h) Olsen, M. T.; Rauchfuss, T. B.; Wilson, S. R. *J. Am. Chem. Soc.* **2010**, *132*, 17733–17740. (i) Barton, B. E.; Rauchfuss, T. B. *J. Am. Chem. Soc.* **2010**, *132*, 14877–14885. (j) Camara, J. M.; Rauchfuss, T. B. *J. Am. Chem. Soc.* **2011**, *133*, 8098–8101. (k) Darensbourg, M. Y.; Lyon, E. J.; Smee, J. J. *Coord. Chem. Rev.* **2000**, *206−207*, 533–561. (l) Zhao, X.; Georgakaki, I. P.; Miller, M. L.; Yarbrough, J. C.; Darensbourg, M. Y. *J. Am. Chem. Soc.* **2001**, *123*, 9710–9711. (m) Mejia-Rodriguez, R.; Chong, D.; Reibenspies, J. H.; Soriaga, M. P.; Darensbourg, M. Y. *J. Am. Chem. Soc.* **2004**, *126*, 12004–12014. (n) Liu, T.; Darensbourg, M. Y. *J. Am. Chem. Soc.* **2007**, *129*, 7008–7009. (o) Tye, J. W.; Lee, J.; Wang, H.-W.; Mejia-Rodriguez, R.; Reibenspies, J. H.; Hall, M. B.; Darensbourg, M. Y. *Inorg. Chem.* **2005**, *44*, 5550–5552. (p) Kaur-Ghumaan, S.; Schwartz, L.; Lomoth, R.; Stein, M.; Ott, S. *Angew. Chem., Int. Ed.* **2010**, *49*, 8033–8036. (q) Schwartz, L.; Eilers, G.; Eriksson, L.; Gogoll, A.; Lomoth, R.; Ott, S. *Chem. Commun.* **2006**, 520–522. (r) Singh, P. S.; Rudbeck, H. C.; Huang, P.; Ezzaher, S.; Eriksson, L.; Stein, M.; Ott, S.; Lomoth, R. *Inorg. Chem.* **2009**, *48*, 10883–10885. (s) Aguirre de Carcer, I.; DiPasquale, A.; Rheingold, A. L.; Heinekey, D. M. *Inorg. Chem.* **2006**, *45*, 8000–8002. (t) Matthews, S. L.; Heinekey, D. M. *Inorg. Chem.* **2010**, *49*, 9746–9748. (u) Capon, J.-F.; Gloaguen, F.; Schollhammer, P.; Talarmin, J. *Coord. Chem. Rev.* **2005**, *249*, 1664–1676. (v) Capon, J. F.; Gloaguen, F.; Pétillon, F. Y.; Schollhammer, P.; Talarmin, J. *Eur. J. Inorg. Chem.* **2008**, *2008*, 4671–4681. (w) Felton, G. A. N.; Petro, B. J.; Glass, R. S.; Lichtenberger, D. L.; Evans, D. H. *J. Am. Chem. Soc.* **2009**, *131*, 11290–11291. (x) Felton, G. A. N.; Vannucci, A. K.; Chen, J.; Lockett, L. T.; Okumura, N.; Petro, B. J.; Zakai, U. I.; Evans, D. H.; Glass, R. S.; Lichtenberger, D. L. *J. Am. Chem. Soc.* **2007**, *129*, 12521–12530. (y) Artero, V.; Fontecave, M. *Coord. Chem. Rev.* **2005**, *249*, 1518–1535.

(4) DuBois, D. L.; Bullock, R. M. *Eur. J. Inorg. Chem.* **2011**, 1017–1027.

(5) (a) Yang, J. Y.; Bullock, R. M.; Rakowski DuBois, M.; DuBois, D. L. *MRS Bull.* **2011**, *36*, 39–47. (b) Wilson, A. D.; Shoemaker, R. K.; Miedaner, A.; Muckerman, J. T.; DuBois, D. L.; Rakowski DuBois, M. *Proc. Natl. Acad. Sci. U.S.A.* **2007**, *104*, 6951–6956. (c) Yang, J.; Chen, S.; Dougherty, W. G.; Kassel, W. S.; Bullock, R. M.; DuBois, D.; Raugei, S.; Rousseau, R.; Dupuis, M.; Rakowski DuBois, M. *Chem. Commun.* **2010**, *46*, 8618–8620. (d) Jain, A.; Lense, S.; Linehan, J. C.; Raugei, S.; Cho, H.; DuBois, D. L.; Shaw, W. J. *Inorg. Chem.* **2011**, *50*, 4073–4085.

(6) Wilson, A. D.; Newell, R. H.; McNevin, M. J.; Muckerman, J. T.; Rakowski DuBois, M.; DuBois, D. L. *J. Am. Chem. Soc.* **2006**, *128*, 358–366.

(7) Pool, D. H.; DuBois, D. L. *J. Organomet. Chem.* **2009**, *694*, 2858–2865.

(8) Kilgore, U.; Roberts, J.; Pool, D. H.; Appel, A.; Stewart, M.; Rakowski DuBois, M.; Dougherty, W. G.; Kassel, W. S.; Bullock, R. M.; DuBois, D. L. *J. Am. Chem. Soc.* **2011**, *133*, 5861–5872.

(9) Appel, A. M.; Pool, D. H.; O'Hagan, M.; Shaw, W. J.; Yang, J. Y.; Rakowski DuBois, M.; DuBois, D. L.; Bullock, R. M. *ACS Catal.* **2011**, *1*, 777–785.

(10) O'Hagan, M.; Shaw, W. J.; Raugei, S.; Chen, S.; Yang, J. Y.; Kilgore, U. J.; DuBois, D. L.; Bullock, R. M. *J. Am. Chem. Soc.* **2011**, *133*, 14301–14312.

(11) Bard, A. J.; Faulkner, L. R. *Electrochemical Methods: Fundamentals and Applications*, 2nd ed.; John Wiley & Sons: New York, 2001.

(12) Wayner, D. D. M.; Parker, V. D. *Acc. Chem. Res.* **1993**, *26*, 287–294.

(13) Fraze, K.; Wilson, A. D.; Appel, A. M.; Rakowski DuBois, M.; DuBois, D. L. *Organometallics* **2007**, *26*, 3918–3924.

(14) Ellis, W. W.; Miedaner, A.; Curtis, C. J.; Gibson, D. H.; DuBois, D. L. *J. Am. Chem. Soc.* **2002**, *124*, 1926–1932.

(15) Galan, B. R.; Schöffel, J.; Linehan, J. C.; Seu, C.; Appel, A. M.; Roberts, J. A. S.; Helm, M. L.; Kilgore, U. J.; Yang, J. Y.; DuBois, D. L.; Kubiak, C. P. *J. Am. Chem. Soc.* **2011**, *133*, 12767−12779.

(16) Berning, D. E.; Miedaner, A.; Curtis, C. J.; Noll, B. C.; Rakowski DuBois, M.; DuBois, D. L. *Organometallics* **2001**, *20*, 1832–1839.

(17) Berning, D. E.; Noll, B. C.; DuBois, D. L. *J. Am. Chem. Soc.* **1999**, *121*, 11432–11447.

(18) Curtis, C. J.; Miedaner, A.; Ellis, W. W.; DuBois, D. L. *J. Am. Chem. Soc.* **2002**, *124*, 1918–1925.

(19) Faviera, I.; Duñach, E. *Tetrahedron Lett.* **2004**, *45*, 3393–3395.

(20) (a) Nicholson, R. S.; Shain, I. *Anal. Chem.* **1964**, *36*, 706–723. (b) Savéant, J. M.; Vianello, E. *Electrochim. Acta* **1965**, *10*, 905–920. (c) Savéant, J. M.; Vianello, E. *Electrochim. Acta* **1967**, *12*, 629–646.

(21) Felton, G. A. N.; Glass, R. S.; Lichtenberger, D. L.; Evans, D. H. *Inorg. Chem.* **2006**, *45*, 9181–9184.

(22) (a) Chen, S.; Raugei, S.; Rousseau, R.; Dupuis, M.; Bullock, R. M. *J. Phys. Chem. A* **2010**, *114*, 12716–12724. (b) Dupuis, M.; Chen, S.; Raugei, S.; DuBois, D. L.; Bullock, R. M. *J. Phys. Chem. A* **2011**, *115*, 4861–4865.

(23) Nimlos, M. R.; Chang, C. H.; Curtis, C. J.; Miedaner, A.; Pilath, H. M.; DuBois, D. L. *Organometallics* **2008**, *27*, 2715–2722.

(24) Raebiger, J. W.; Miedaner, A.; Curtis, C. J.; Miller, S. M.; Anderson, O. P.; DuBois, D. L. *J. Am. Chem. Soc.* **2004**, *126*, 5502–5514.

(25) Kaljurand, I.; Kütt, A.; Soovälli, L.; Rodima, T.; Mäemets, V.; Leito, I.; Koppel, I. A. *J. Org. Chem.* **2005**, *70*, 1019–1028.

(26) Hathaway, B. J.; Holah, D. G.; Underhill, A. E. *J. Chem. Soc.* **1962**, 2444–2448.

(27) Märkl, V. G.; Jin, G. Y.; Schoerner, C. *Tetrahedron Lett.* **1980**, *21*, 1409–1412.

(28) Ochida, A.; Hamasaka, G.; Yamauchi, Y.; Kawamorita, S.; Oshima, N.; Hara, K.; Ohmiya, H.; Sawamura, M. *Organometallics* **2008**, *27*, 5494–5503.